FloEFD simulation of micro-turbine engine

T.V. Trebunskikh, A.V. Ivanov, G.E. Dumnov
Mentor Graphics, Moscow, Russia

Keywords: micro-turbine engine, CFD, combustion, compressor, turbine

Abstract

Turbojet engines have complex geometry and physics of processes occurring in them. Understanding these processes is very important for designing of a high-performance product. It is very difficult to investigate some processes inside of an engine during the tests. In such conditions CFD methods become an extremely useful tool.

A computational study of internal flow in KJ 66 micro-turbine engine calculated as one unit is presented. The calculations are made with multiCAD-embedded CFD tool FloEFD at several rotational speeds (rotation of air in the compressor and the turbine, conjugate heat transfer, air/kerosene combustion are taken into account).

The main results of simulation are presented. Some parameters are compared with experimental data. Thereby it is shown that predicted temperature at the outlet of the compressor and the combustion chamber, mass flow at the inlet of the engine and thrust of the engine have good agreement with experimental data. Rather nonuniform distribution of fluid temperature at the outlet of the combustion chamber is observed that can negatively affect the turbine performance.

Nomenclature

c	specific heat
c_p	specific heat at constant pressure
C_μ, $C_{\varepsilon 1}$, $C_{\varepsilon 2}$	turbulent constants
d	minimum distance from a wall
e	$= c \cdot T$, specific internal energy
$\vec{\mathbf{g}}$	vector of gravity
h	$= c_p \cdot T$, enthalpy
h_m^0	individual thermal enthalpy of m^{th} component
H	total enthalpy
$\bar{\bar{\mathbf{I}}}$	unit tensor
k	turbulent kinetic energy
K	reaction rate parameter
m	molar mass
M	pseudo molecules
P	static pressure
P'	effective pressure
P_{ref}	reference value of pressure
Pr	Prandtl number
Pr_t	turbulent Prandtl number
Q_H	specific heat release (or absorption) per unit volume
r	distance from a point to the rotational axis in the rotational reference frame
$\bar{\bar{\mathbf{s}}}$	shear stress tensor
S_T	volume heat source
Sc	Schmidt number
Sc_t	turbulent Schmidt number
t	time
T	temperature

$\vec{\mathbf{U}}$	vector of velocity
$\vec{\mathbf{x}}$	radius vector
y	concentration
y_m	concentration of mth component
y_O , y_F	mass fraction of oxidizer and fuel residue respectively
Y_F	mass fraction of the fuel
Z_P	mass fraction of the combustion “product”
ε	turbulent dissipation rate
μ	dynamic viscosity
μ_t	turbulent viscosity
λ_i	eigenvalues of the thermal conductivity tensor
ρ	density
ρ_{ref}	reference value of density
σ_k , σ_ε	turbulent constants
$\bar{\bar{\boldsymbol{\tau}}}^R$	Reynolds stress tensor
$\bar{\bar{\boldsymbol{\tau}}}^\Sigma$	summarized stress tensor
$\vec{\boldsymbol{\Omega}}$	vector of angular velocity

Subscripts

F	fuel
O	oxidizer
P	product

1. Introduction

Micro-turbine engines have been developed for specific flight applications. They have been used in unmanned aerial vehicles (UAVs), which were designed for short flight duration. A lot of different kinds of UAVs are now operating worldwide. Another common application for small gas turbines is an auxiliary power unit (APU) supplementing aircraft engines which provide additional power when required[1,2]. Because of the small size micro-turbine engines show small mass flow rates of air, low pressure ratios, but very high rotational speeds. A micro-turbine engine chosen for the study is KJ 66 (Fig.1), which is one of the most robust small engines with available design.

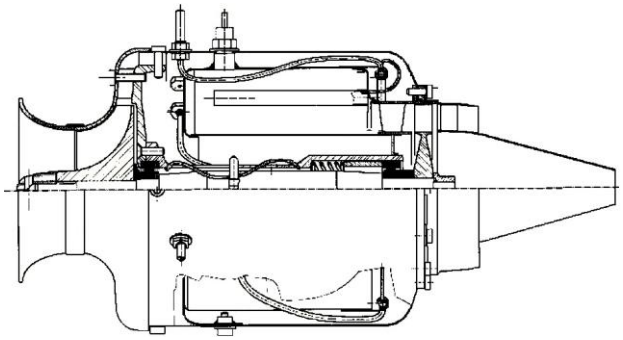

Figure 1. The scheme of KJ 66 micro-turbine engine.

Complex geometry and small size of this kind of engines limit the access of conventional instruments for the measurement of flow parameters which is needed for better understanding of a complex flow structure. Also choosing optimal design of single parts of an engine during tests is rather expensive procedure. In such conditions CFD methods become an extremely useful tool. Results demonstrated in this paper are obtained in multiCAD-embedded full-featured general purpose CFD tool FloEFD serving the needs of popular MCAD systems.

Several authors investigated KJ 66 engine but they calculated it as separate parts. Thereby nonuniformity of parameters between main parts of the engine (e.g. velocity and pressure distribution at the inlet of the combustion chamber) is not taken into account in that approach. In

this paper a computational study of internal flow in KJ 66 micro-turbine engine calculated as a whole unit is presented. According to this approach more accurate results are obtained.

In the first part of the paper, the statement of the problem including description of boundary conditions and mesh is presented. In the next section modelling approach is described including governing equations, rotational and combustion models. In the third section main results of calculation of all engine part are presented and compared to experimental data[1-3]. Major conclusions are listed in the last section.

2. Statement of the problem

KJ 66 micro-turbine engine is a high-performance model jet engine that has been well known since its introduction.

The compressor is a turbocharger wheel with the diameter of 0.066 m. The compressor's diffuser is made of aluminum which blades have the form of fat wedges. The axial turbine wheel has 23 blades that can stand extremely high rotational speeds. The combustion chamber is compact, so that the short shaft can be used. KJ 66 engine weighs around 0.95 kg depending on the version and offers a very good thrust to weight ratio[1]. The combustion chamber features direct injection of fuel through six vaporizing sticks for achieving complete combustion before the turbine.

The model of the engine was built in SolidWorks CAD system and demonstrated in Fig. 2 and the real prototype is shown in Fig. 3. This engine is calculated as one unit (360 degrees without transferred, symmetrical or periodic conditions).

Figure 2. The model of KJ 66 engine in FloEFD.

Figure 3. The real prototype.

Several mesh variants with the total cells' number of ~600000, ~3500000, ~9000000 are examined. The local initial mesh was created on all main parts of the engine such as the compressor, the combustion chamber, the turbine and so on. The additional local mesh on all blade's surfaces was specified (Fig. 4).

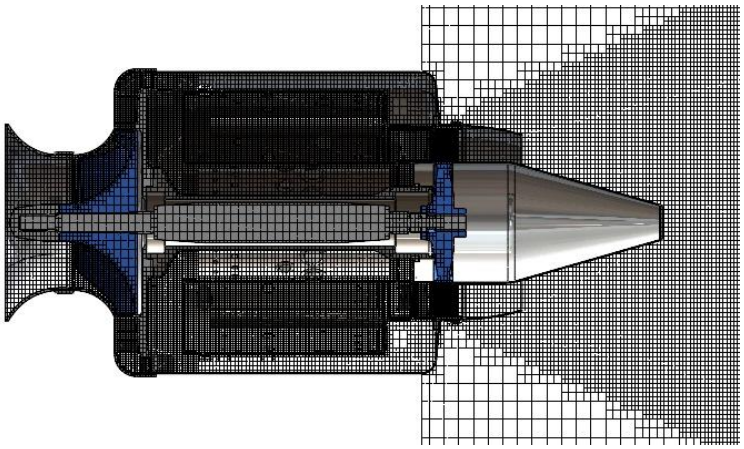

Figure 4. The calculation mesh of KJ 66 engine model with ~3500000 cells.

Five cases with rotational speeds of 40000, 60000, 80000, 100000 (the nominal mode) and 120000 rpm are considered here. Specifying of local rotational zones in FloEFD is shown in Fig. 5.

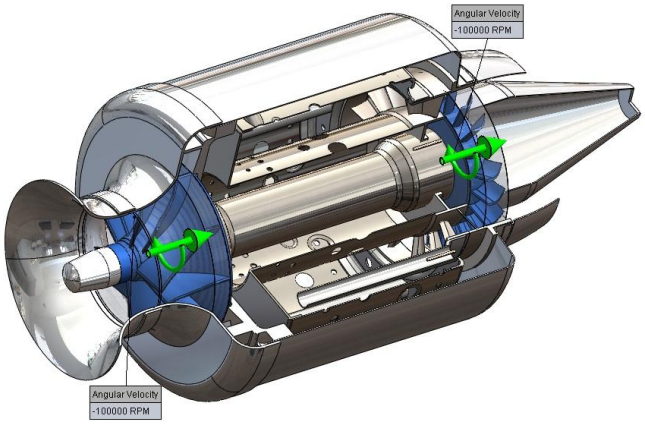

Figure 5. The rotational regions of KJ 66 engine.

The total pressure and the static temperature of air are 101325 Pa and 288.15 K respectively at the inlet of the engine. At the outlet the same conditions are treated as atmospheric ones. The static temperature of kerosene is 300 K at the outlets of the fuel sticks and mass flow depends on the rotational speed. Kerosene is specified as a gas phase. The air fuel ratio is ~65.

The solid parts are specified as aluminum, steel and inconel for consideration of conjugate heat transfer. Initial temperature of solid parts, which was obtained in the preliminary calculations, is specified. The radiation in the combustion chamber is not taken into account because of investigation of general characteristics of the engine.

The calculation is provided in the transient regime with the time step 0.0001 s. In the solids time step equals 0.01 s until establishing of the flow.

The combustion is calculated using equilibrium approach with two models – the model of non premixed combustion and the model of premixed combustion with the limited combustion rate.

3. Modelling approach

3.1. Governing equations

FloEFD solves the Favre-averaged Navier-Stokes equations, which are formulations of mass, momentum and energy conservation laws for fluid flows with modified k-ε turbulent model with the damping functions proposed by Lam and Bremhorst[4] and with the laminar/ turbulent transition.

The governing equations for all dependant variables can be written in the general form:

$$\frac{\partial(\rho\Phi)}{\partial t}+\nabla\cdot\left(\rho\vec{\mathbf{U}}\Phi\right)=\nabla\cdot\left(\Psi\right)+\mathrm{S}\,. \tag{1}$$

Table 1. The dependant variables with the corresponding transport coefficients and the source terms.

Φ	Ψ	S
1	0	0
$\vec{\mathbf{U}}$	$\bar{\bar{\boldsymbol{\tau}}}^{\Sigma}$	$-\nabla P'+\frac{1}{2}\rho\nabla\left(\Omega^2 r^2\right)+\left(\rho-\rho_{ref}\right)\vec{\mathbf{g}}-2\rho\left(\vec{\boldsymbol{\Omega}}\times\vec{\mathbf{U}}\right)$
H	$\vec{\mathbf{U}}\bar{\bar{\boldsymbol{\tau}}}^{\Sigma}+\left(\lambda+\lambda_t\right)\nabla T-\left(\frac{\mu}{\mathrm{Pr}}+\frac{\mu_t}{\mathrm{Pr}_t}\right)\sum_m h_m\nabla y_m+\left(\mu+\frac{\mu_t}{\sigma_k}\right)\nabla k$	S_{T}
y	$\left(\frac{\mu}{\mathrm{Pr}}+\frac{\mu_t}{\mathrm{Pr}_t}\right)\nabla y$	0
k	$\left(\mu+\frac{\mu_t}{\sigma_k}\right)\nabla k$	$\bar{\bar{\boldsymbol{\tau}}}^{R}\nabla\cdot\vec{\mathbf{U}}-\rho\varepsilon$
ε	$\left(\mu+\frac{\mu_t}{\sigma_\varepsilon}\right)\nabla\varepsilon$	$\frac{\varepsilon}{k}\left(f_1\mathrm{C}_{\varepsilon 1}\bar{\bar{\boldsymbol{\tau}}}^{R}\nabla\cdot\vec{\mathbf{U}}-f_2\mathrm{C}_{\varepsilon 2}\rho\varepsilon\right)$

$$P'=P-\mathrm{P}_{ref}-\rho_{ref}\vec{\mathbf{g}}\vec{\mathbf{x}}+\frac{2}{3}\rho k\,, \tag{2}$$

$$\bar{\bar{\boldsymbol{\tau}}}^{\Sigma}=\left(\mu+\mu_t\right)\bar{\bar{\mathbf{s}}}\,,\ \bar{\bar{\boldsymbol{\tau}}}^{R}=\mu_t\bar{\bar{\mathbf{s}}}-\frac{2}{3}\rho k\bar{\bar{\mathbf{I}}} \tag{3}$$

$$\bar{\bar{\mathbf{s}}} = \nabla \cdot \vec{\mathbf{U}} + \left(\nabla \cdot \vec{\mathbf{U}}\right)^T - \frac{2}{3}\nabla \cdot \vec{\mathbf{U}}\bar{\bar{\mathbf{I}}}\,, \tag{4}$$

$$H = h + \frac{\vec{\mathbf{U}}^2}{2} - \frac{1}{2}\Omega^2 r^2 + \frac{5}{3}k - \sum_m h_m^0 y_m\,, \tag{5}$$

$$\mu_t = \mathrm{C}_\mu f_\mu \frac{\rho k^2}{\varepsilon}\,, \tag{6}$$

$$f_\mu = \left(1 - \exp\left(-0.0165 R_d\right)\right)^2 \left(1 + \frac{7.5}{\mathrm{Re}_t}\right),\ f_1 = 1 + \left(\frac{0.05}{f_\mu}\right)^3,\ f_2 = 1 - \exp\left(-\mathrm{Re}_t^2\right), \tag{7}$$

$$R_d = \frac{\rho\sqrt{k}d}{\mu},\ \mathrm{Re}_t = \frac{\rho k^2}{\mu\varepsilon} \tag{8}$$

$$\mathrm{C}_\mu = 0.09,\ \mathrm{C}_{\varepsilon 1} = 1.44,\ \mathrm{C}_{\varepsilon 2} = 1.92,\ \mathrm{Pr}_t = 0.9,\ \sigma_k = 1,\ \sigma_\varepsilon = 1.3. \tag{9}$$

To describe turbulent boundary layers with approach “Two-Scale wall functions”[5] Van Driest’s universal profiles are employed in FloEFD: the near wall function and the subgrid model of boundary layer. This approach allows FloEFD to overcome a traditional CFD code restriction of having a very fine mesh density near walls in a calculation domain.

3.2. Rotational modelling approach

The local rotating zones are used for analysis of the fluid flow in the model[4]. In accordance with the employed approach, each rotating solid component is surrounded by an axisymmetrical rotating zone, which has its own coordinate system rotating together with the component. The fluid flow equations in the non-rotating zones of the computational domain are solved in the non-rotating Cartesian Global Coordinate System. To connect solutions obtained within the rotating zones and in the non-rotating part of the computational domain, special internal boundary conditions are set automatically at the fluid boundaries of the rotating zones.

3.3. Combustion modelling

FloEFD can consider the thermal effects of chemical reactions related to the combustion of gas-phase mixtures[4]. The model implemented in FloEFD refers to the equilibrium approach to consideration of combustion products, where several substances mixed up to the molecular level react instantly until the chemical equilibrium is achieved. Thermodynamical properties of individual substances which occur in this system are determined from the maximum entropy condition of the isolated system at the implementation of the conservation laws of atoms, energy and electrically neutral statement[6]. This approach does not provide ability to calculate the combustion of the premixed mixtures.

The limited combustion rate option extends the equilibrium model in case of premixed combustion. The conventional single reaction irreversible mechanism is introduced for this approach:

$$M_O + M_F \xrightarrow{K} M_P\,, \tag{10}$$

where $K = f(T)$ is a reaction rate parameter, which depends on temperature.

The product that appears in the reaction is transferred over a fluid region in accordance with the following equation:

$$\frac{\partial\left(\rho Z_P\right)}{\partial t} + \nabla \cdot \left(\rho \vec{\mathbf{U}} Z_P - \left(\frac{\mu}{\mathrm{Sc}} + \frac{\mu_t}{\mathrm{Sc}_t}\right)\nabla Z_P\right) = m_P \rho \frac{\left(1 - Z_P\right)^2}{m_O m_F}\left(1 - Y_F\right) Y_F K\,. \tag{11}$$

In this model the equation of state has the following form:

$$h\left(T, P, Y_F, Z_P\right) = y_O h_O + y_F h_F + y_P h_P\,, \tag{12}$$

$$\rho\left(T, P, Y_F, Z_P\right) = \left(\frac{y_O}{\rho_O} + \frac{y_F}{\rho_F} + \frac{y_P}{\rho_P}\right)^{-1}, \tag{13}$$

$$y_O = \left(1 - Y_F\right)\left(1 - Z_P\right),\ y_F = Y_F\left(1 - Z_P\right),\ y_P = Z_P\,. \tag{14}$$

3.4. Conjugate Heat Transfer

FloEFD allows predicting simultaneous heat transfer in solid and fluid media with energy exchange between them. Heat transfer in fluids is described by the energy conservation

equation[4]. The phenomenon of anisotropic heat conductivity in solid media is described by the following equation:

$$\frac{\partial(\rho e)}{\partial t} = \nabla \cdot (\lambda_i \nabla T) + Q_H \,. \tag{15}$$

Media considered here are isotropic so that $\lambda_1 = \lambda_2 = \lambda_3 = \lambda$.

4. Results

In this section results of KJ 66 micro-turbine engine calculation are presented. The results of this simulation are compared with experimental data. Despite the calculation of the whole engine it is more convenient to investigate FloEFD results by dividing them into four groups: the compressor, the combustion chamber, the turbine calculations and general results.

4.1. Compressor

KJ 66 micro-turbine engine uses a compressor wheel from a car turbocharger[7]. This wheel is coupled to a wedge diffuser in the engine as it is shown in Fig. 6.

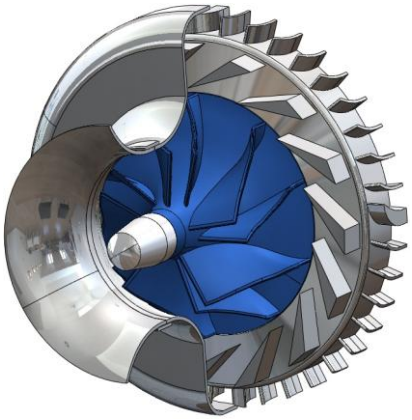

Figure 6. The compressor and the diffuser of KJ 66 engine.

Figure 7 shows flow trajectories colored by velocity magnitude and pressure distribution on surfaces of the compressor and the diffuser at the normal mode. Pressure on the compressor's blades can be lower than 65000 Pa and can reach 180000 Pa on the diffuser's blades. Pressure distribution in compressor's sections at the normal mode can be seen in Fig. 8.

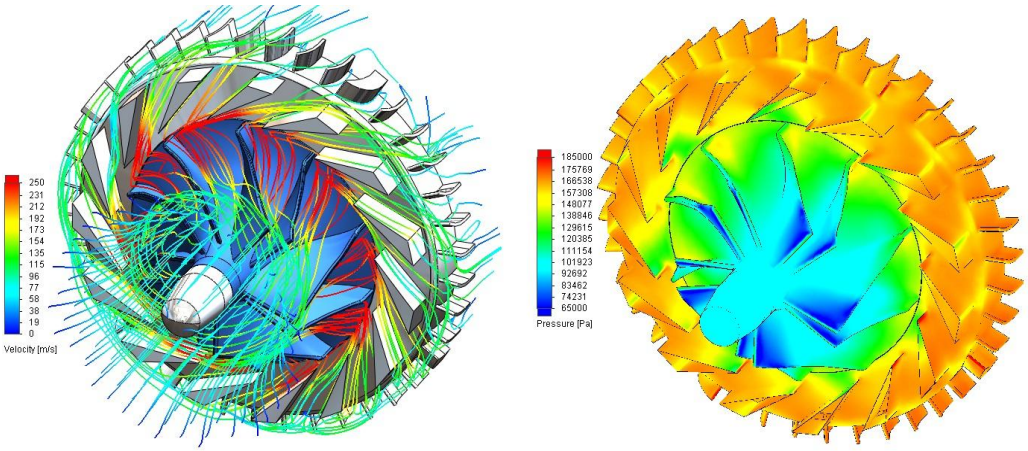

Figure 7. Flow trajectories colored by velocity magnitude (left) and pressure distribution on surfaces of the compressor and the diffuser (right) at normal mode.

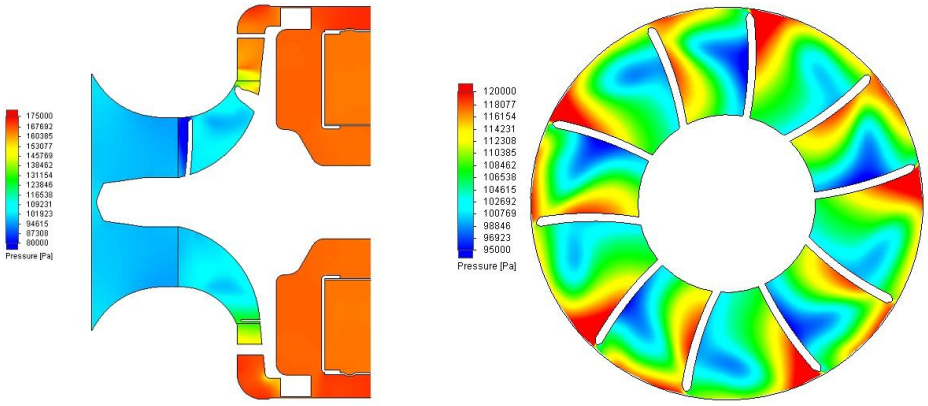

Figure 8. Pressure distribution at the longitudinal section (left) and the cross section (right) at normal mode.

In Fig. 9 air mass flow at the inlet of the engine at various rotational speeds of the compressor can be seen. The FloEFD results are compared with experimental data from Kamps T.[(1)] The values of mass flow match good experimental data and almost do not depend on cells' number. As for efficiency of the compressor it was obtained that this part has rather low efficiency for such type of compressors of micro-turbine engines. The large source on inefficiency is located in the wedge diffuser.

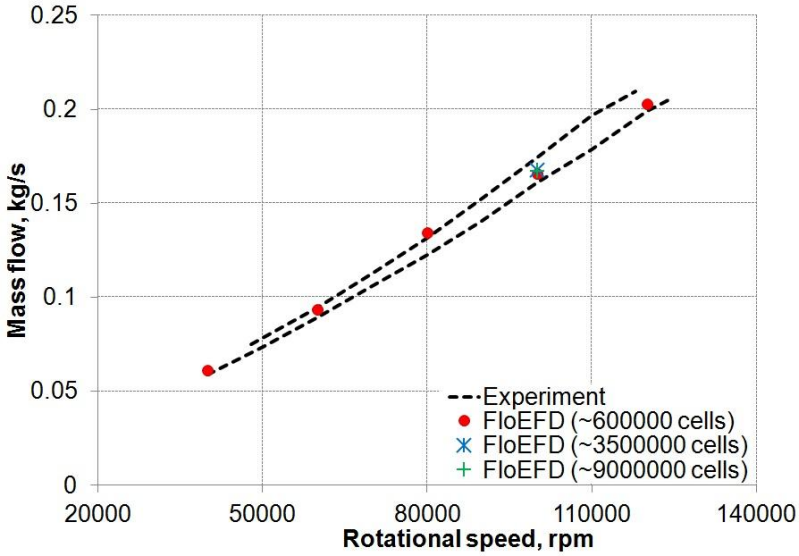

Figure 9. Air mass flow at the inlet of KJ 66 engine.

4.2. Combustion chamber

The combustion chamber of KJ 66 engine features direct fuel injection through 6 vaporizing sticks to ensure complete combustion inside the chamber. The combustion chamber's model is shown in Fig. 10.

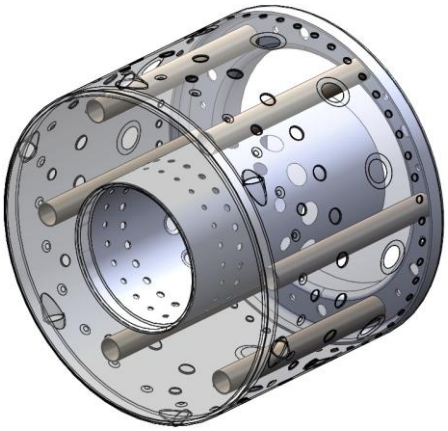

Figure 10. The combustion chamber of KJ 66 engine.

It should be noted that both approaches of the combustion model (see p.3.3) used in this simulation do not show significant distinctions. Thereby the results indicated here relate to the non premixed combustion approach. Figure 11 shows flow trajectories colored by velocity magnitude and pressure distribution on internal and blade's surfaces of the NGV at the normal mode.

Fig. 12 displays fluid temperature and velocity distributions at two longitudinal sections of the combustion chamber with flow vectors at the normal mode. Temperature in the combustion chamber reaches ~2400 K. Increasing of velocity in the zones of holes of the combustion chamber is observed especially on the rear wall of it. Rather nonuniform fluid temperature distribution at the outlet of the combustion chamber can be seen in Fig. 13. Temperature gradients at this section have a negative influence on the performance of the turbine and, as a result, this fact can lead to lifetime reduction of it.

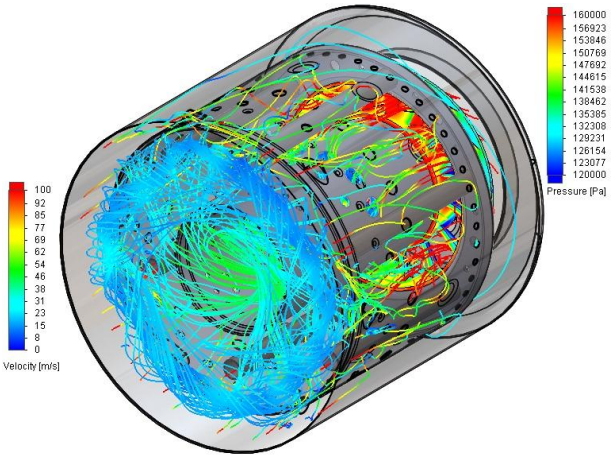

Figure 11. Flow trajectories colored by velocity magnitude and pressure distribution on internal and blade's surfaces of the NGV at the normal mode.

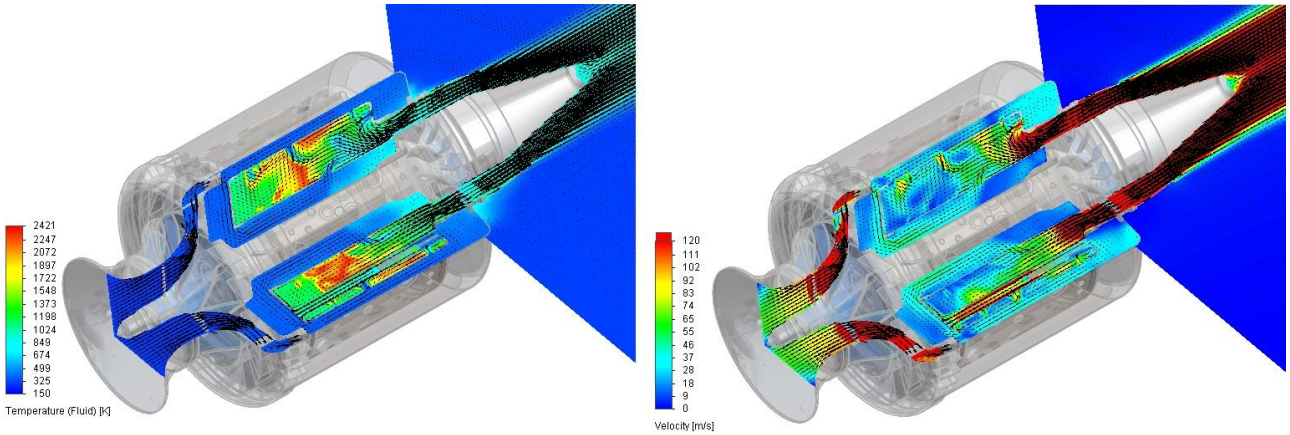

Figure 12. Fluid temperature (left) and velocity (right) distributions at two longitudinal sections of the combustion chamber with flow vectors at the normal mode.

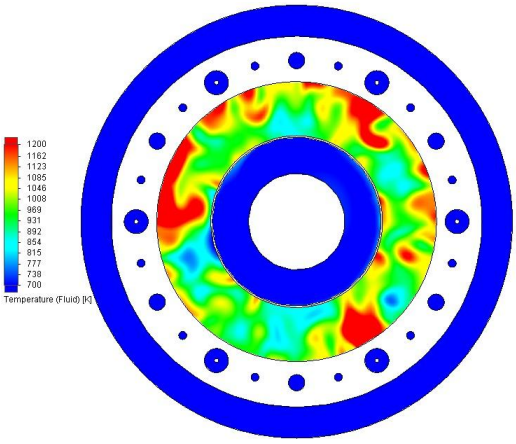

Figure 13. Fluid temperature distribution at the outlet of the combustion chamber.

Figures 14 and 15 show comparison of temperature and fuel mass fraction distribution in the combustion chamber at 120000 rpm obtained in FloEFD and Fluent presented by C.A. Gonzales, K.C. Wong and S. Armfield[2]. The FloEFD model is simplified as well as the Fluent model (examining not all parts of the engine) but all features of the combustion chamber are taken into account. The symmetry conditions are not used in FloEFD model as opposed of Fluent model. So there are some differences in distribution of parameters can be seen in these figures. Basically FloEFD and Fluent results have a good agreement taking into account points listed above. It is clearly visible in Fig. 14 that primary combustion zone is located in the central part of the chamber. It can be seen in Fig. 15 that at the outlet of the combustion chamber fuel mass fraction equals ~0.02.

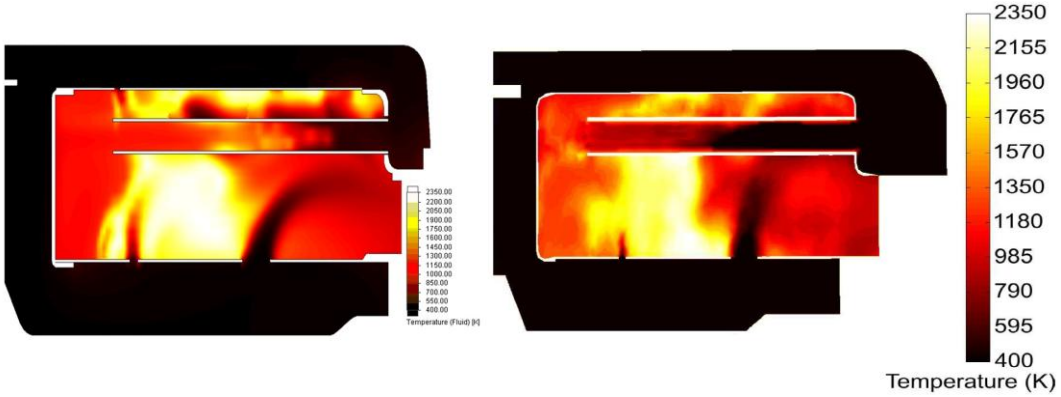

Figure 14. Temperature distribution in the combustion chamber at 120000 rpm obtained in FloEFD (left) and Fluent[2] (right).

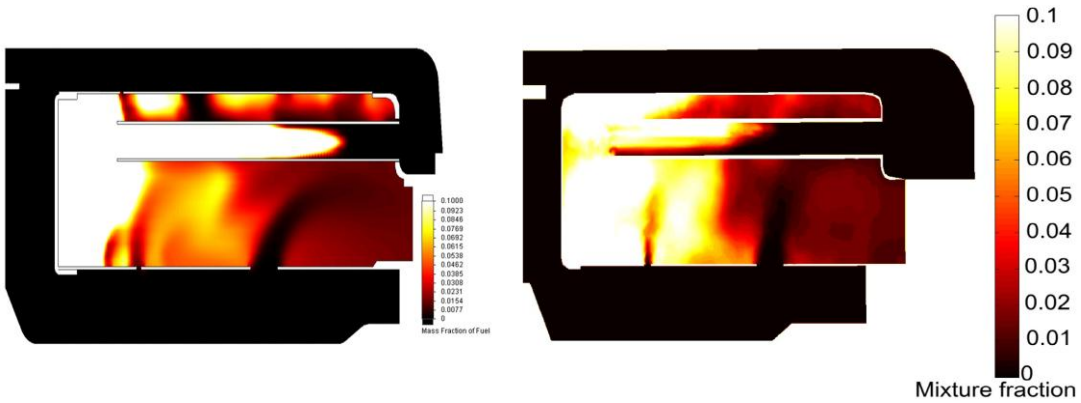

Figure 15. Fuel mass fraction distribution in the combustion chamber at 120000 rpm obtained in FloEFD (left) and Fluent[2] (right).

Figure 16 shows temperature and fuel mass fraction distribution in the combustion chamber at 120000 rpm obtained in FloEFD where all features of whole KJ 66 micro-turbine engine are examined. In this figure it can be seen that distributions of temperature and fuel mass fraction have some difference from previous pictures due to taking into account the NGV (nozzle guide vanes) that leads to increase of speed at the outlet of the combustion chamber.

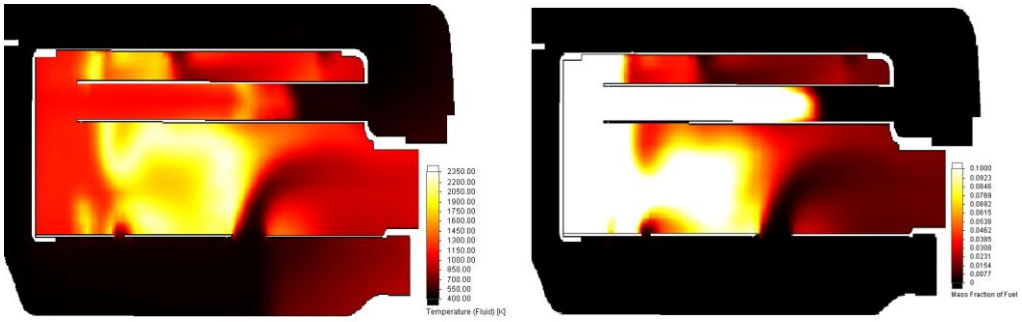

Figure 16. Temperature (left) and fuel mass fraction (right) distributions in the combustion chamber at 120000 rpm obtained in FloEFD (the NGV is taken into account).

FloEFD allows exporting some parameters as loads for structural and thermal analyses to Creo Elements/Pro Mechanica. Surface temperature was exported for thermal calculation. Then the structural analysis was provided using temperature which was a result of that calculation and pressure which was exported from FloEFD. Figure 17 shows displacement distribution of structural analysis. The combustion chamber is deformed under loads and displacement can reach 0.001 m.

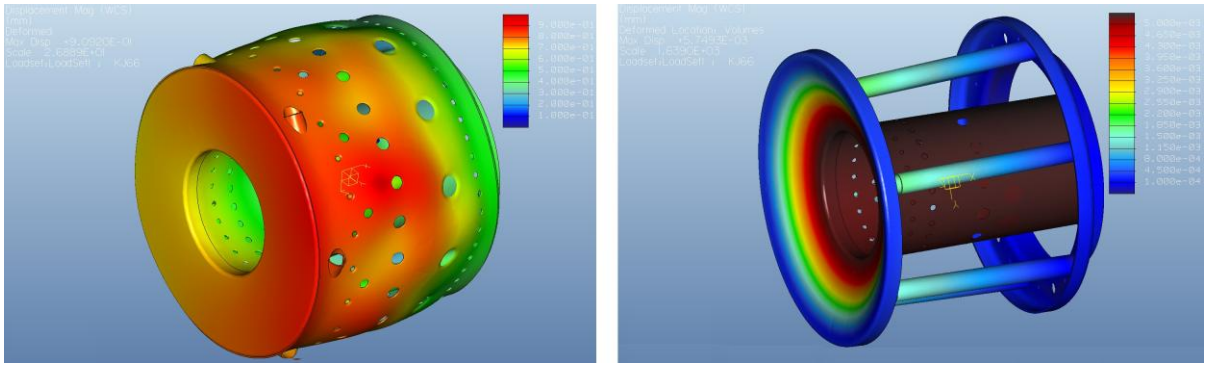

Figure 17. Displacement distribution on surfaces of the combustion chamber in Creo Elements/Pro Mechanica (scaling 20%).

4.3. NGV and turbine

The turbine wheel is made of 0.006 m thick stainless steel or inconel depending on modification. The blades are twisted and profiled manually. The models of the NGV and the turbine are shown in Fig. 18.

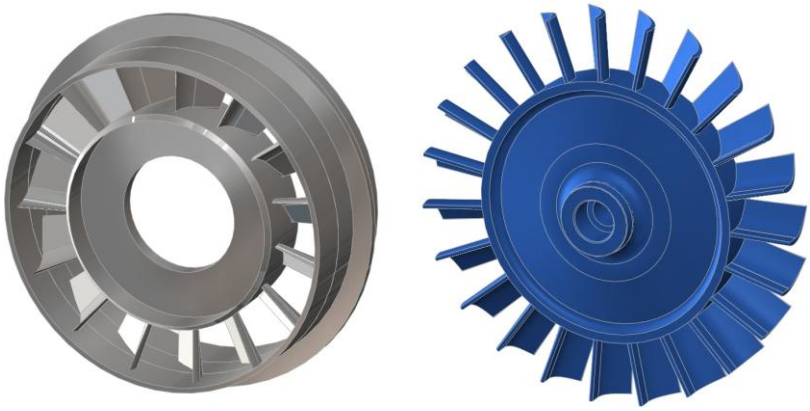

Figure 18. The NGV (left) and the turbine (right) of KJ 66 engine.

Pressure distribution at a section of the NGV and the turbine and temperature distribution on the turbine's blades at the normal mode are presented in Fig. 19. During the passage of flow through the NGV and turbine pressure drops from 160000 Pa to 110000 Pa. Spread of temperature values reaches 100 K on the turbine's blades that can lead to rather strong deformation of them.

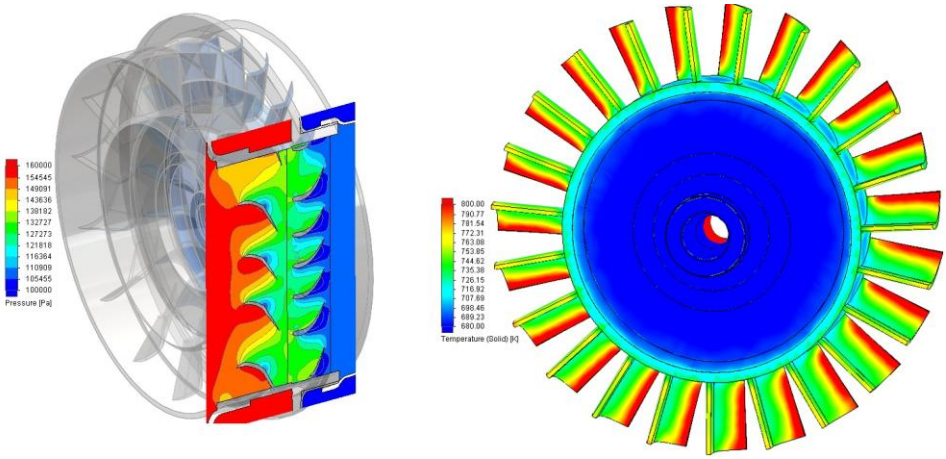

Figure 19. Pressure distribution at a section of the NGV and the turbine (left) and temperature distribution on the turbine's blades at the normal mode.

4.4. General results

General results of FloEFD prediction are provided in this section. Figure 20 shows flow trajectories colored by velocity magnitude. Pressure distribution on surfaces of the engine and velocity distribution near surfaces of the engine are presented in Fig. 21.

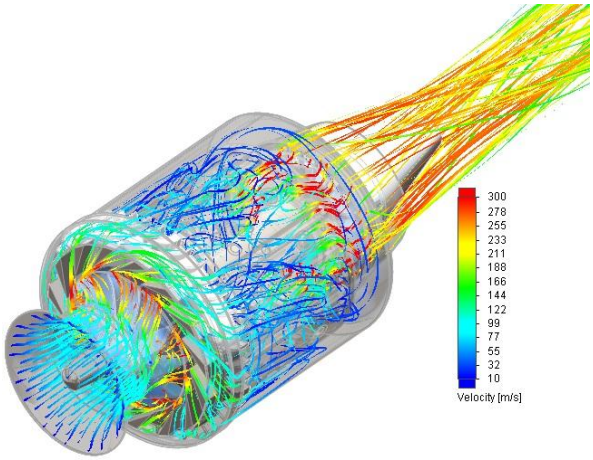

Figure 20. Flow trajectories colored by velocity magnitude.

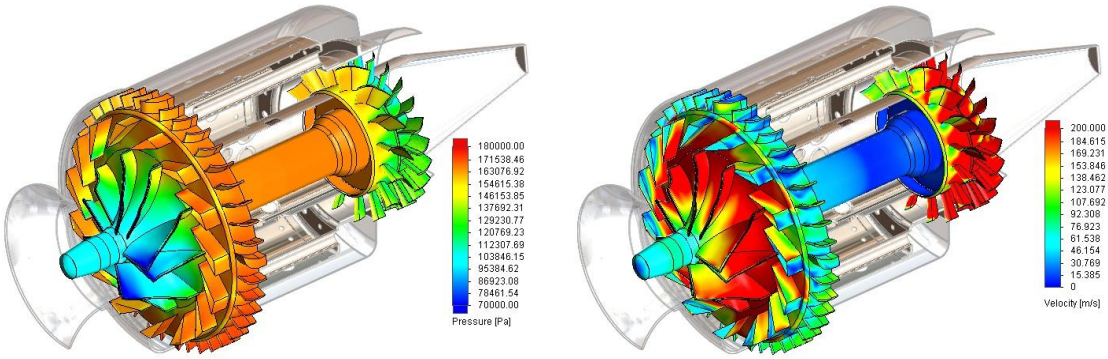

Figure 21. Pressure (left) and velocity (right) distributions.

In Fig. 22 predicted and experimental temperature magnitudes at the outlet of the diffuser, at the outlet of the combustion chamber and at the outlet of the engine at different modes can be seen. The predicted and measured[1,2] temperatures at the outlet of the compressor at 120000 rpm have very close values. At the outlet of the combustion chamber at modes up to 80000 rpm value of mean temperature equals ~930 K and at the normal mode and 120000 rpm – ~990 K. At 120000 rpm predicted mean temperature has 1.6% discrepancy with experimental data.

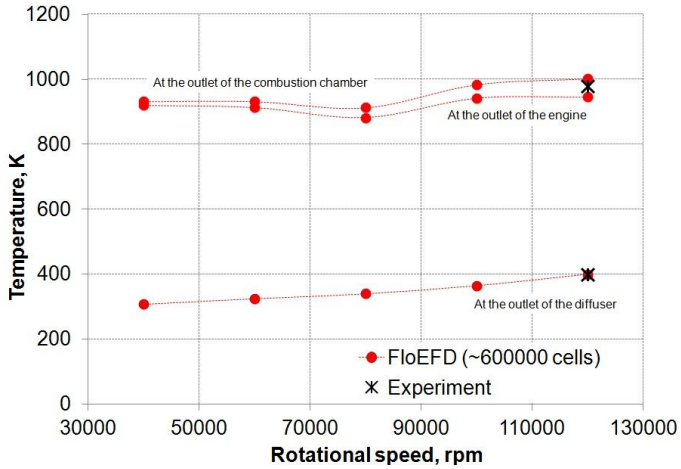

Figure 22. Temperature at the outlet of the diffuser, the combustion chamber and the engine.

Figure 23 shows comparisons of measured[1] and predicted values of thrust of KJ 66 engine at different modes. It can be seen that experimental and predicted values have a good agreement up to 80000 rpm and at 100000 rpm some discrepancy from experimental data is observed. Possible

reason of this divergence can be deformation of engine's parts at high rotational speeds. This deformation is not taken into account in this investigation.

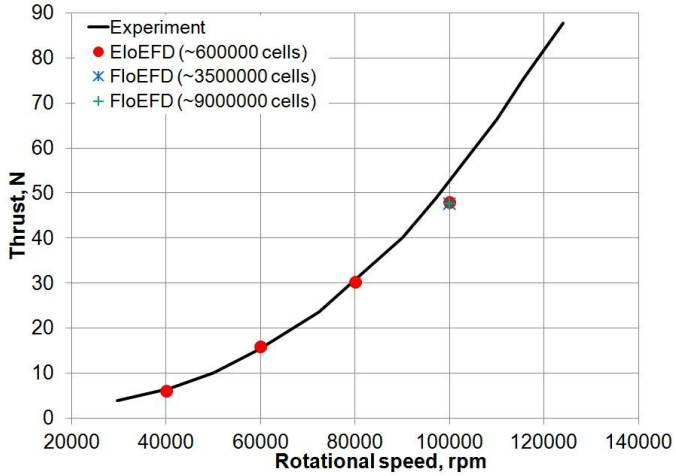

Figure 23. Thrust of KJ 66 engine.

Comparison of predicted values of torque of the compressor and the turbine of KJ 66 engine with different cell numbers is presented in Fig. 24 where a good agreement between each other is observed. As the compressor and the turbine are on the same shaft it means that moment produced by the turbine is enough for supporting specified rotational speed of the compressor's wheel. Thereby the engine is in the operation condition. It can be seen at normal mode that the higher cell number, the better agreement between torques, e.g. discrepancy is ~ 4% for ~600000 cells and ~0.8% for ~9000000 cells.

It can be noted that there is mesh convergence in this task. All parameters are similar in all considered cases of cell numbers. Thereby mesh of ~600000 cells is enough for definition almost all integral parameters here.

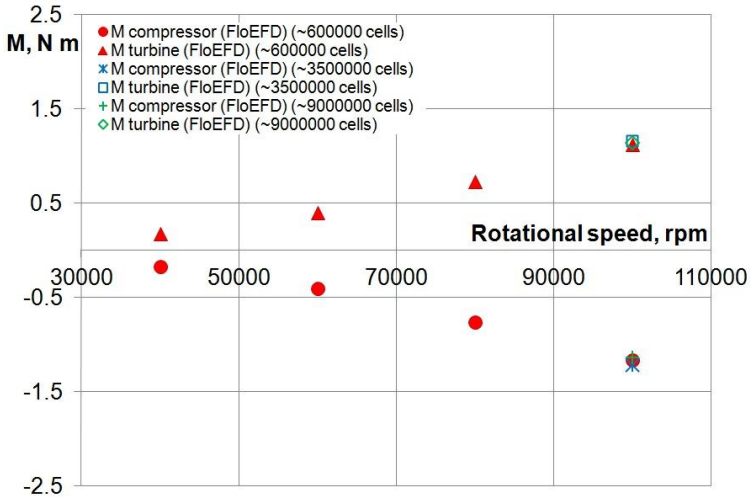

Figure 24. Torques of the compressor and the turbine of KJ 66 engine.

5. Conclusions

1. The CFD analysis of KJ 66 micro-turbine engine, which is calculated as one unit without any transferred, symmetrical and periodical conditions between its parts in FloEFD software is presented in this paper. Also it is shown how to provide thermal and structural analyses in Creo Elements/Pro Mechanica using CFD results as temperature and pressure loads. As the whole engine in transient regime is calculated so unsteady effects of a stator-rotor interaction, unsteady heat transfer of the turbine's blades can be taken into account and the quality of the simulation can be improved due to unsteady combustion.
2. Comparisons of measured and predicted values of the main integral parameters such as air mass flow at the inlet of the engine, thrust, temperatures at the outlet of the diffuser and at the outlet of the combustion chamber show a good agreement. Also it can be seen a good

agreement between calculations in FloEFD and Fluent for appropriate model of the engine (some parts of the engine are not taken into account). Moreover change of the flow pattern due to taking into account all parts of the KJ 66 engine is shown here. Mesh convergence is presented for this calculation. All parameters are similar in all considered cases of cell numbers so that mesh of ~600000 is enough in this task for definition almost all integral parameters. Thereby FloEFD allows providing series of “what-if” CFD analyses with rather small mesh and export data for structural and thermal analyses.

3. Complicated zones of KJ 66 engine are shown and the causes of their occurrence are examined:

   3.1. The compressor of this engine has the rather low efficiency for such type of compressors of micro-turbine engines. The large source on inefficiency is located in the wedge diffuser.

   3.2. Rather nonuniform distribution of fluid temperature at the outlet of the combustion chamber is observed. It can negatively affect on the performance of the turbine.

   3.3. Maximum value of temperature on the internal rear wall of the housing of the engine can reach 750 K.

   If these points are taken into account the engine can be modified for better performance.

References

1. Kamps, T. Model jet engines, UK, 2005.
2. Gonzalez, C.A., Wong, K.C., Armfield S. Computational study of a micro-turbine engine combustor using large eddy simulation and Reynolds average turbulence models, Austral Mathematical Soc, Australia, 2008.
3. Schreckling, K. Home built model turbines, UK, 2005.
4. FloEFD Technical Reference, Mentor Graphics Corporation, 2011.
5. Enhanced turbulence modeling in FloEFD, Mentor Graphics Corporation, 2011.
6. Volkov, V.A., Ivanov, A.V., Streltsov, V.U., Khokhlov, A.V. Using of equilibrium models for calculation of gas combustion, 5th Russian National Conf of Heat Exchange, Moscow, Russia, 2010.
7. Verstraete, D., Hendrick, P., Djanali, V., Gonzalez, C., Ling, J., Wong, K.C., Armfield, S. Micro propulsion activities at the university of Sydney, Australia.
8. Gonzalez, C.A., Wong, K.C., Armfield, S. A computational study of the influence of the injection characteristics on micro-turbine combustion, 16th Austral. Fluid Mechanics Conf, Australia, 2007.
9. Ling, J., Wong, K.C., Armfield, S. Numerical Investigation of a Small Gas Turbine Compressor, 16th Austral. Fluid Mechanics Conf, Australia, 2007.